SRTTU

JCARME
ISSN: 2228-7922

Journal of Computational and Applied Research
in Mechanical Engineering
Vol. 7, No. 2, pp. 151-160
jcarme.srttu.edu

Comparison of three different numerical schemes for 2D steady incompressible lid-driven cavity flow

S. Gharahjeh [a], A. Ashraf [a] and G. Mahtabi [b,*]

[a]Hydraulic division, Middle East Technical University, Ankara, 06800, Turkey
[b]Department of Water Engineering, University of Zanjan, Zanjan, 45371-38791, Iran

Article info:
Received: 05/06/2016
Accepted: 17/10/2017
Online: 09/01/2018

Keywords:
Convergence criterion,
Implicit solution,
Primitive variable,
Vorticity.

Abstract
In this study, a numerical solution of 2D steady incompressible lid-driven cavity flow is presented. Three different numerical schemes were employed to make a comparison on the practicality of the methods. An alternating direction implicit scheme for the vorticity-stream function formulation, explicit and implicit schemes for the primitive variable formulation of governing Navier-Stokes equations were attempted. A fairly fine uniform grid was adopted for all the cases after a technical procedure was applied to come up with the proper mesh size that would make the solution roughly independent of mesh quality. The solutions obtained for different Reynolds numbers are presented and compared. Superiority of numerical approaches was investigated and compared to benchmark solutions available in the literature. Based on the results of the present research, it can be claimed that explicit scheme used for primitive variable formulation can be only half the way (as in R_e=2500 for explicit to R_e=5000 for ADI and implicit schemes) as successful as the other two numerical methods due to its relative simplicity.

Nomenclature

A	Bottom surface of cavity, m^2	$\Delta x = \Delta y$	Grid size, m
cs	Control surface, m^2	y^+	Non-dimensional wall distance
cv	Control volume, m^3	**Greek letters**	
N	Number of grid nodes	$\forall$	Volume, m^3
R	Residual	ξ	Vorticity
R_e	Reynolds Number	ν	Kinematic Viscosity, m^2/s
P	Pressure, N/m^2	ρ	Density, kg/m^3
x, y	x and y coordinate respectively, m	ω	Over relaxation parameter
t	Time, s	ψ	Stream function
u, v	x and y velocity respectively (m/s)	**Subscripts**	
U, V	x and y velocity along the vertical centerline respectively,	*i, j*	Number of mesh in x and y directions respectively
u^+	Non-dimensional velocity	**Superscripts**	
U_o	Constant velocity, m/s	*n*	Number of time step
U_*	Shear stress velocity, m/s		

**Corresponding author*
email address: ghmahtabi@gmail.com

1. Introduction

Lid-driven cavity flow is considered as one of the most studied problems in the field of computational fluid dynamics (CFD) due to its simple geometry and the fluid inside retaining all the flow physics. The flow is confined from all four sides and is a case of a recirculating flow prompted by the moving the top lid with the other three walls at rest. Lid-driven cavity flow is also considered as a benchmark for testing numerical efficiency and accuracy of different numerical methods [1].

A number of the research papers related to the flow in a driven cavity may be divided into two categories, i.e. the physical side of the flow and confirmation of the newly evolved numerical schemes [2]. Most of the flow pattern studies inside the cavity pertain to the steady state, but very few studies focused on the mechanisms of transients until the steady state is achieved [3]. For low Reynolds numbers, most of the numerical methods show similar results but as the Reynolds number starts increasing, results are different from each other. Also, some researchers predict that the flow remains steady at high Reynolds number while others show that the flow is unsteady.

Peng et al. [4] investigated transition process in a square lid-driven cavity from laminar to chaotic flow. They found out that the flow remains steady up to R_e=7402 and then as Reynolds number increases to 11000, the flow is in a transition phase after which it is finally routed to chaotic flow for Reynolds number greater than 11000. Bruneau and saad [5] - through numerical simulations- investigated the boundaries of steady state solution for high Reynolds numbers in a square cavity. They observed that steady solution is unstable at R_e=10000. They identified a large vortex with two secondary vortices in the bottom left and right corners for R_e=1000 and a secondary and tertiary vortex in the bottom left corner.

There has so far been no solid agreement in CFD community over the transient Reynolds number at which flow turns into turbulent. Ghia et al. [6] employed the vorticity-stream function formulation of the 2D incompressible Navier-Stokes equations to investigate the affectivity of coupled strongly implicit multigrid (CSI-MG) method for determining the high-R_e fine-mesh flow solutions in square cavity flows. Results were obtained for configurations with Reynolds number as high as 10000 and mesh size of 257×257. Barragy and Carey [7] showed calculations for the 2D driven cavity incompressible flow problem. A p-type finite element scheme for the fully coupled stream Function-Vorticity formulation of the Navier-Stokes equations was used. To show the vortex flow features in detail and minimize the impact of corner singularities, graded meshes were used. They observed that for the R_e up to 12500, steady state solutions can be maintained.

Zdanski et al. [8] performed a numerical simulation to study the comparison between laminar and turbulent flows over shallow cavities and examined the effect of Reynolds number, aspect ratio and inlet turbulence level on turbulent flow. They observed that with increasing Reynolds number the center of the laminar structure of vortex is decreased. By contrast, the center of both large and small structures for turbulence case was seen to be unchanged. Erturk [1] studied lid-driven cavity flow using physical, mathematical and numerical methods in detail and suggested that for very high Reynolds numbers finer grids are important for the resolution of the flow. At R_e=7500, the quaternary vortex at the bottom left corner was observed indicating an improvement over previous results. Kumar et al. [9] simulated a lid-driven cavity flow using a multigrid method full approximation scheme. The main conclusion of the study was that it is possible to obtain solutions with higher order discretization on a very fine grid by using the multigrid method. Moshkin and Poochinapan [10] developed a new finite-difference scheme to solve the 2D Navier-Stokes equations in the lid-driven cavity flow. The results obtained in all test cases were in excellent agreement with other established numerical results.

Poochinapan [11] introduced a finite difference scheme to treat nonlinear convective terms in the stream function formulation and applied to the flow in the lid-driven cavity. The results showed that the internal iteration technique performs

robustly and allows one to accurately follow the flow patterns. Yapici and Uludag [12] presented computer simulation results (a non-uniform version of the QUICK scheme) of steady incompressible flow in a 2D square lid-driven cavity up to R_e=65000. The results demonstrated that discretization of the flow field by using a non-uniform mesh structure increased the accuracy and non-oscillatory solutions at high R_e. Salah Uddin and Saha [13] investigated numerically the lid-driven cavity flow with wavy bottom surface. They examined the effects of R_e, the number of undulations and the grid size on numerical solutions of streamlines. The results showed that the wall undulation has an effect upon the flow in the lid-driven square cavity. By using the number of undulations at the bottom surface of a cavity, the skin friction increased. Marioni et al. [14] used a variational multiscale finite element approach to solve a conducting fluid inside a two-dimensional square domain. The study focused on a high magnetic interaction parameter range and high R_e. An expression to calculate the maximum time step that guarantees convergence in explicit schemes was presented and validated through numerical tests.

In the present paper, the attempt is to make a robust comparison over the extent to which three different but major numerical algorithms of solving cavity problem can be applied. In addition, algorithms for solving the governing equations are explained in a more down to detail fashion as of an instructive vessel. With all this, the computer codes and discretization procedure can be supplied for the avid reader upon request.

2. Material and method

2.1. Numerical methods for solution

2.1.1. Alternating direction implicit method (ADI)

It is usually convenient to adopt the vorticity (ξ) transport and stream function (ψ) formulation of Navier-Stokes equations for two-dimensional plane flows. The governing equations are as follows:

$$\frac{\partial^2 \psi}{\partial x^2}+\frac{\partial^2 \psi}{\partial y^2}=-\xi \tag{1}$$

$$\frac{\partial \xi}{\partial t}+\frac{\partial (u\,\xi)}{\partial x}+\frac{\partial (v\,\xi)}{\partial y}=\nu\left(\frac{\partial^2 \xi}{\partial x^2}+\frac{\partial^2 \xi}{\partial y^2}\right) \tag{2}$$

In order to solve the ξ and ψ , a numerical approach is required. Many algorithms exist in the literature; the one method suitable for the condition is the alternating direction implicit method (ADI) for vorticity transport equation and point successively over-relaxation (PSOR) method for stream function equation. The type of discretization for the vorticity transport equation is forward time central space differences (FTCS) as shown in Eq. (3). Also, the convective terms have to undergo first-order upwind.

$$\frac{\xi_{i,j}^{n+1/2}-\xi_{i,j}^{n}}{\Delta t}=u_{i,j}^{n}\frac{\xi_{i+1,j}^{n}-\xi_{i-1,j}^{n}}{2\Delta x}+v_{i,j}^{n}\frac{\xi_{i,j+1}^{n}-\xi_{i,j-1}^{n}}{2\Delta y}= \nu\left[\frac{\xi_{i+1,j}^{n}-2\xi_{i,j}^{n}+\xi_{i-1,j}^{n}}{(\Delta x)^2}+\frac{\xi_{i,j+1}^{n}-2\xi_{i,j}^{n}+\xi_{i,j-1}^{n}}{(\Delta x)^2}\right] \tag{3}$$

In the ADI method, $\xi_{i,j}^{n+1/2}$ is unknown that is to be explicitly determined from a previous step of $\xi_{i,j}^{n}$ in either of primary directions (initial value of $\xi_{i,j}^{n=1}$ can be assumed). Then, the entire step is marched towards $\xi_{i,j}^{n+1}$ (final solution) using the solution available from a previous time step in the other direction normal to the initial direction, that is, $\xi_{i,j}^{n+1/2}$.

The stream function is a Poisson type differential equation which is solved via the SOR algorithm. The finite difference discretization -with 2nd order accuracy- of the equation is written as:

$$\frac{\psi_{i+1,j}-2\psi_{i,j}+\psi_{i-1,j}}{\Delta x\,\Delta x}-\frac{\psi_{i,j+1}-2\psi_{i,j}+\psi_{i,j-1}}{\Delta y\,\Delta y}=-\xi_{i,j} \tag{4}$$

The solution is followed by the calculation of residuals and substitution of it in the point successive over relaxation formula to compute the point wise stream function all over the flow domain. For $\Delta x=\Delta y=\Delta$:

$$R_{i,j}=\frac{1}{4}\left[\psi_{i+1,j}+\psi_{i-1,j}+\psi_{i,j+1}+\psi_{i,j-1}-\Delta^2\xi_{i,j}-4\psi_{i,j}^{n}\right] \tag{5}$$

$$\psi_{i,j}^{n+1}=\psi_{i,j}^{n}+\omega R_{i,j} \tag{6}$$

where ω is an over relaxation parameter that accelerates the convergence of the iterations. The value of ω is dependent on the mesh size, geometry of the flow domain and the boundary conditions. The optimum value of the ω was determined as 1.93 through a different approach. The method used for determination of ω value has been shown in Fig. 1. In this figure, *N* is the number of grid nodes in each direction over the flow domain and *N*=130 was decided after careful observations of numerical independency on grid size for *N*=130 (more explanation in part 3). It is noteworthy that the curves overlap on top of one another after *N* exceeds 101, thus the Curve for *N*=130 has not been shown to avoid confusion while the value of ω is absolutely the same as that of *N*=101.

In Fig. 1, error specified on the vertical axis is an overall space average error over the computational domain and is the summation of differences between the exact and numerical solution of the Poisson equation for a variety of the mesh configurations.

2.1.2. Primitive variables (u, v, P) explicit formulation

The following equations are continuity and momentum balance in primary directions in integral form (same as Navier-Stokes equations):

$$\frac{\partial}{\partial t}\int_{cv} u d\forall + \int_{cs} uV\ dA = \int_{cs} \nu \nabla u\ dA - \int_{cv} \frac{1}{\rho}\frac{dp}{dx} d\forall \quad (7)$$

$$\frac{\partial}{\partial t}\int_{cv} v d\forall + \int_{cs} vV\ dA = \int_{cs} \nu \nabla v\ dA - \int_{cv} \frac{1}{\rho}\frac{dp}{dy} d\forall \quad (8)$$

$$\int_{cs} V\ dA = 0 \quad (9)$$

In Eq. (7), the first term from left-hand side is called the local term (or unsteady term), and the 2nd is convective term. On the right-hand side of the equation (Eq. (7)), the first term is named viscous damping responsible for resistance to flow and the rightmost one is the source term. On the right-hand side of the equation (Eq. (7)), the first term is named viscous damping responsible for resistance to flow and the rightmost one is the source term. Finite volume on the uniform rectangular grid with 2nd order accuracy has been used to discretize and integrate the governing equations over a control volume. The control volume has been shown in Fig. 2 which shows the staggered discretization with dependent variables on it.

The time-dependent momentum equations in two primary directions are solved explicitly for the velocity field. The local time-dependent terms are handled in a time-marching trend iteratively to reach stability which implies that the discrete solution of (*u*-*v*-*P*) coming from an earlier time step is used in place of the next iteration as long as old and new primitive variables change no more with respect to time pass. That is, u^{n+1} is first calculated based on u^n and then in the second iteration, u^{n+1} is used in place of u^n to come up with the updated u^{n+1}. This trend goes on so long as $u^{n+1}$and u^n are nearly equal. By looking at the discretized unsteady term of Navier-Stokes equations, same understanding can be achieved where u^{n+1} is replaced by un in a proceeding time step until convergence as:

$$\frac{\partial}{\partial t}\int_{cs} u d\forall = \frac{u_{i,j}^{n+1} - u_{i,j}^{n}}{\Delta t}\Delta x\,\Delta y \quad (10)$$

To prevent solution instabilities, the first-order upwind method has been used for convective terms. Upwind effectively takes into account the propagation of information on the flow field by either back or forward differencing the convective terms based on flow direction. Continuity equation has undergone a major manipulation to be converted into pressure equation. It is noteworthy that discrete pressure is located at the cell center with velocity sitting all around it to build up a staggered uniform grid as shown in Fig. 2. Again for the pressure equation, SOR algorithm has been used with an over-relaxation value of 1.7. Same termination criteria were used for this case as the ADI.

2.1.3. Primitive variables (u, v, P) implicit formulation

For the implicit solution of the equations, Ansys Fluent the commercial code (licensed by Middle East Technical University (METU)) was used.

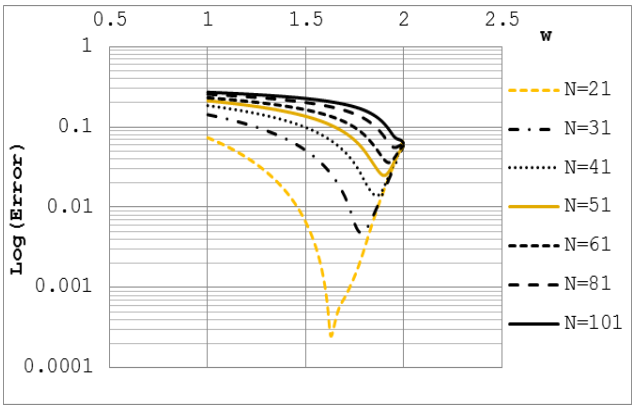

Fig. 1. Determination of the optimal ω value.

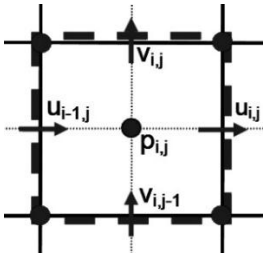

Fig. 2. The finite volume cell with discrete primitive variables.

When a straight calculation of the dependent variables cannot be made in terms of known quantities, the computation is said to be implicit. The equations under investigation (Eqs. (7-9)) are nonlinear and include the calculation of three unknowns at a time.

Despite the fact that implicit formulation scheme corresponds to a set of linear equations which can be solved directly, Fluent makes use of iterative algorithms towards a final solution. Iterations are carried out to advance a solution through a series of steps from a starting state to a final stage named as the converged state. As a matter of fact, the iteration steps often do not demonstrate a realistic time-dependent behavior. In fact, this aspect of the implicit scheme makes it appeal for steady state computations, because the number of iterations needed for a solution is usually much smaller than the number of time steps required for a precise transient which asymptotically approaches towards steady state.

2.2. Boundary conditions

Application of boundary conditions for the cavity problem can be fallen into two types, the stationary walls and the moving lid. As long as the stationary wall is concerned, the no-slip boundary condition has to be implemented. For the vorticity stream function formulation, boundary condition has to be specified for both stream function and vorticity as such:

2.2.1. Stationary walls

Stream function takes a constant value on the wall which is adopted as zero in this problem. For vorticity transportation, Eq. (1) needs to be solved on the wall. By employing proper measures, the boundary condition can be computed as below:

$$\xi_{wall}^{n} = \frac{2(\xi_{wall}^{n} - \xi_{adjacent\ to\ wall}^{n})}{\Delta x \Delta x} + O(\Delta x) \qquad (11)$$

where $O(\Delta x)$ is equated to zero since 2nd order accuracy of discretization has been used. The value of vorticity is exact on the wall and no interpolation is required. The boundary condition for the primitive variable formulation

is rather different since the staggered grid prevents the coincidence of no-slip boundary condition with the grid itself. The no-slip boundary condition needs to be imposed as such:

$$u_{(Next\ to\ the\ wall-Within\ flow\ domain)} = -u_{(Next\ to\ the\ wall-Outside\ flow\ domain)} \quad (12)$$

$$v_{(Next\ to\ the\ wall-Within\ flow\ domain)} = -v_{(Next\ to\ the\ wall-Outside\ flow\ domain)} \quad (13)$$

Equations (12, 13) are nothing but no-slip conditions at a point (wall) that is located between two grid points and interpolating comes in hand.

2.2.2 Moving wall

For the boundary condition of moving wall, suppose that the cavity lid moves with a constant velocity of U_o. Again by solving the Eq. (1) and making use of Taylor series expansion along with certain manipulations following relation can be yield:

$$\xi^n_{Moving\ wall} = \frac{2(\xi^n_{wall} - \xi^n_{adjacent\ to\ wall})}{\Delta y\,\Delta y} - \frac{2U_0}{\Delta y} \quad (14)$$

For the implementation of the boundary condition on the moving lid in primitive variable formulation, the average of the velocities in the vicinity of the lid must be equated to the velocity of the moving lid.

$$u_{(Within\ flow\ domain)} + u_{(Outside\ flow\ domain)} = 2U_0 \quad (15)$$

$$v_{(At\ the\ lid)} = 0 \quad (16)$$

2.3. Grid quality

For determination of grid quality, either previous studies should have been used or a systematic approach can reveal this. Normally, when one is solving a laminar flow there is almost no control over the selection of grid size since the rate of strain is linearly related to the shear stress and wall shear stress can be computed linearly with relative ease ($y^+=u^+$). The finer the mesh, the more details of flow can be captured. The wall functions (used for turbulent flows) which are to include the effect of roughness on the boundary can, however, be used to identify the best grid quality for a given problem. The trick to bear in mind is that in the turbulent flows the first grid beside the wall must fall in the validity zone of the wall functions (minimum y^+=30, fully turbulent region). This is because the wall shear stress and consequent velocity distribution are computed according to that first velocity next to the wall which comes from wall functions. In this problem, the grid size is chosen as 130 in both directions. Wan et al. [15] developed a discrete singular convolution (DSC) solver for the driven cavity flow and concluded that the numerical solution is essentially grid independent as the mesh reaches 129×129. Salah Uddin and Saha [13] considered a base grid (125×125 grid points) as the best grid for the computational procedure of driven cavity flow. From literature, it is known that U_*/U=0.04. If U_* can be known, then the y^+=30 can be satisfied [16]. To stay on the safe side the lid velocity was selected as 10 m/s and was replaced into the y^+ relation to yield 133 (or rounded value of 130) number of grids for each direction.

3. Results and discussion

The commercial code Fluent has been used for the solution of the implicit formulation of governing equations. For the solution of vorticity-stream function equations and solution of the explicit formulation of primitive variable equations of motion, codes are developed and run in FORTRAN. Some technical information can be seen in Table 1 regarding the R_e=2500. The results of the runs show that no difference exists between the three different numerical solutions up to a limiting Reynolds number of nearly 2500. With increasing the lid velocity above the limiting Reynolds number, the explicit numerical solution starts to fall apart of the other two algorithms.

In Fig. 3, the streamline patterns exhibit the formation of counter-rotating secondary vortices which appears as the Reynolds number increases. The secondary vortices occur at the right and left bottom corners of the cavity. Also,

the third secondary eddy appears slightly near the upstream top corner [9]. Salah Uddin and Saha [13] investigated the lid-driven cavity flow with a wavy bottom surface and reported that for zero, first and second undulation, large recirculation in the clockwise direction occur in the bottom right and bottom left corner. Also, they observed that in low values of R_e, v-velocity along the horizontal line through the cavity slightly affect near the left and right wall but there is no notable effect on the u-velocity profile. This can be seen in Fig. 3 where the third vortex has not been identified correctly by the explicit method while the other methods are almost giving identical results. As a matter of fact, the explicit solution has reached its stability edge at this Reynolds number while the third vortex can continuously appear and vanish as the oscillatory simulation goes on.

Convergence is when the numerical solution has reached its optimum state and can be no more improved. For every numerical solution, there exist certain convergence criteria based on which iteration towards solution may have to be terminated. The present method for termination of the iterations of this numerical approach is based on monitoring the changes occurring in velocity field. That is, the overall value of mean velocity gets no more changes relative to one step iteration behind. To quantify this change, termination criteria were chosen. As a rule of thumb and according to numerous trials, termination criteria were chosen (for example, see Table 1).

It is noteworthy that the smaller the value of this criteria, the longer and more expensive the computations. Convergence condition for vorticity-stream function solution is to stop iterations when maximum stream function value changes no more than 10^{-6} within an iteration.

Table 1. Details of runs for the different numerical schemes in R_e=2500.

Numerical algorithm	Lid force (N)	Iteration number	Convergence criteria
Vorticity-Stream	0.011467	35620	0.000001
Explicit *u-v-P*	0.011856	59276	0.000001
Implicit *u-v-P*	0.012401	4048	0.001& 0.0001

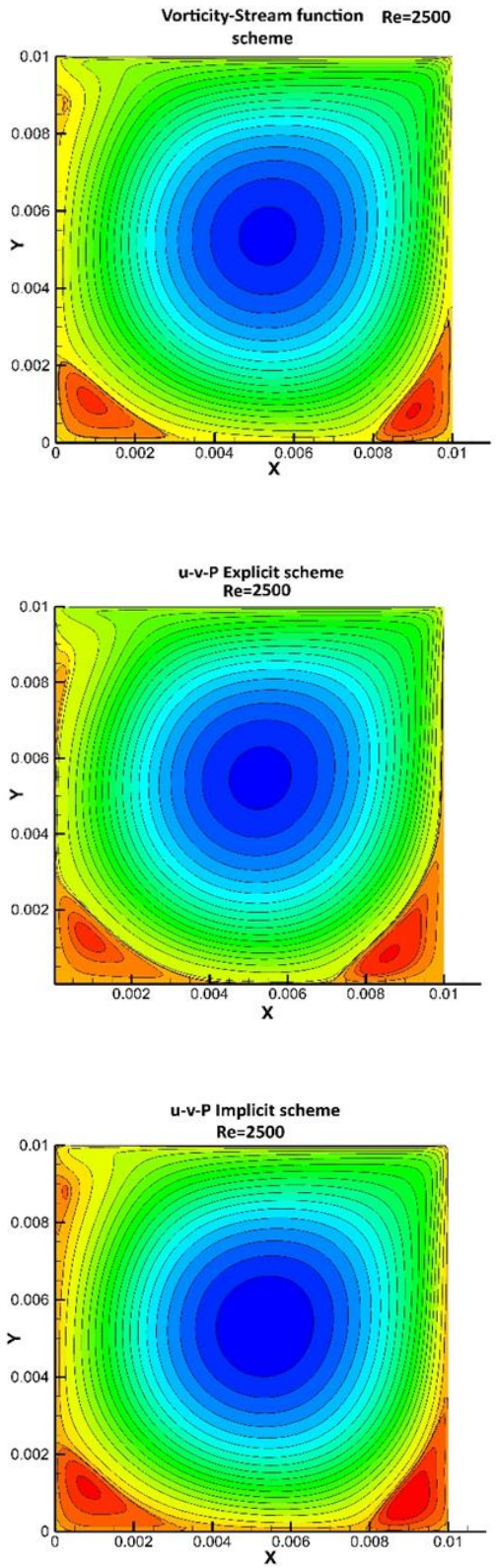

Fig. 3. Comparison of solutions for R_e=2500.

For an explicit primitive variables solution, a criterion is to stop iterations when the mean velocity field value changes no more than 10^{-6} within an iteration. Finally, convergence criteria for the fluent were adopted as 0.0001 for x and y momentum equations and 0.001 for continuity equation. These criteria are usually chosen as a rule of thumb for Fluent which is the indication of a change in the absolute values of mean variables by no more than 0.0001 and 0.001 within an iteration. The residuals and convergence state has also been shown in Fig. 4 for the Fluent run.

Comparison of different numerical schemes for R_e=5000 is given in Table 2 and Fig. 5. After the R_e =2500, the separation starts to become vivid between the implicit solution and vorticity-stream function solution as well. The 3rd vortex next to the back of the lid calculated in ADI (alternating direction implicit) cannot keep pace with the enlarging speed of that of the implicit method. Although the ADI method can handle R_e=5000 with no signs of instability, the solution is not as accurate as that of the implicit method as well as the benchmark solutions available in the literature. This is due to the strength of implicit formulation scheme based on its complexity.

These results have good agreement with the results of Erturk et al. [17], Poochinapan [11] and Salah Uddin and Saha [13]. As the Reynolds number increases, the relative size of secondary eddies in the bottom left and bottom right corner increases. Also, the third secondary eddy develops and enlarges at the top left of the cavity as well. In the implicit solution, the small tertiary vortex at the bottom right of cavity become visible for R_e =5000.

It must be noted that the claims of the present paper hold valid as long as grid quality is kept constant as in all three cases discussed (N=130). On the other hand, according to some literature research, signs of transition to turbulence are observed when Reynolds number reaches 6000 to 8000 and when a grid mesh with less than 257×257 points is used in cavity flow computer simulation, the solution starts to oscillate around Reynolds number range of 7500 to 12500 [1]. The same was verified in the implicit solution of R_e=7500 as shown in Fig. 6.

Table 2. Details of runs for the different numerical schemes in R_e=5000.

Numerical algorithm	Lid force (N)	Iteration number	Convergence criteria
Vorticity-stream	0.0573	36695	0.000001
Explicit *u-v-P*	-	-	-
Implicit *u-v-P*	0.0515	1544	0.001 & 0.0001

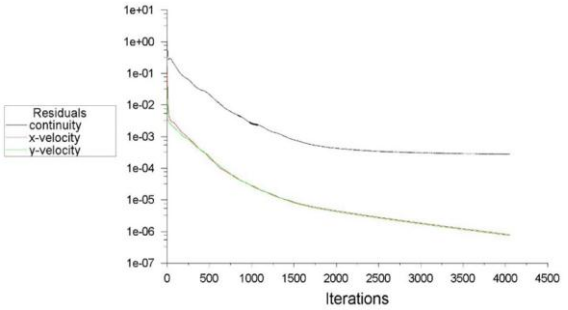

Fig. 4. Residual plot for R_e=2500.

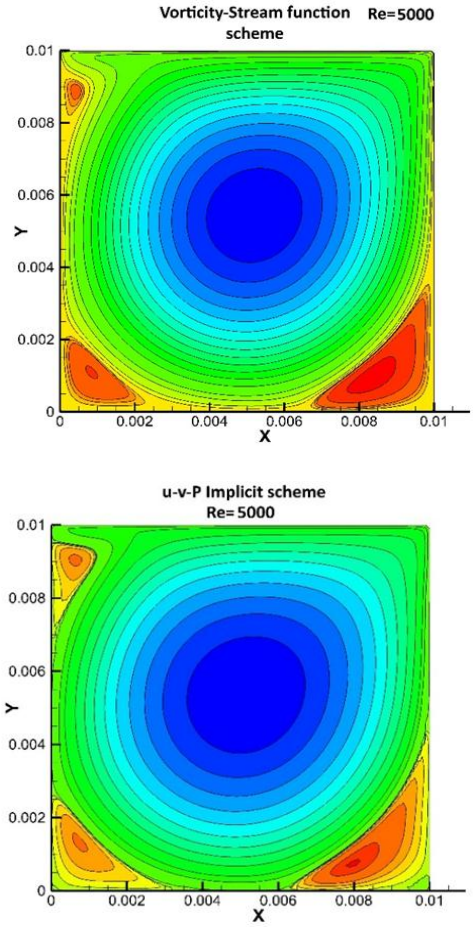

Fig. 5. Comparison of solutions for R_e=5000.

Although the flow field and number of vortices are similar to the benchmark solutions available in the literature, the convergence is suffering a steady state as seen in Fig. 7. With all this, Erturk and Gokcol [18] increased the R_e number to 20000 -obtaining a steady state condition- by using a very fine mesh of 1025×1025 with a fairly sophisticated numerical method. The results clearly show the thinning of the wall boundary layers with increase in R_e, although the rate of this thinning is very slow for $R_e \geq 5000$ [9]. Kumar et al. [9] indicated that changes in u and v velocities are almost linear in the core of a primary vortex as R_e increases. This would indicate that the vorticity is uniform in the region. Also, the tertiary vortex at the bottom left corner grows in size for R_e = 7500. Kumar et al. [9] also reported the augmentation of the tertiary vortices with the increase in the Reynolds number.

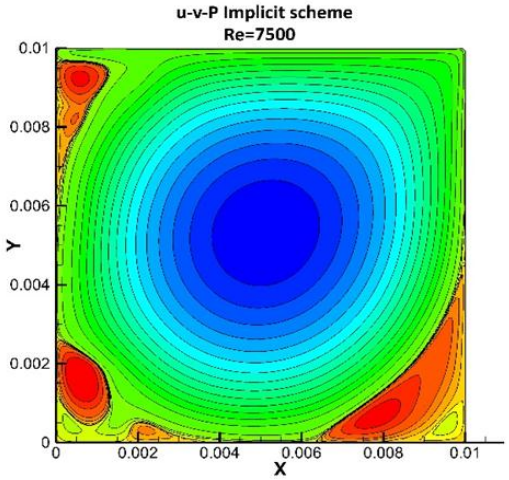

Fig. 6. Result of Implicit *u-v-P* solution for R_e=7500.

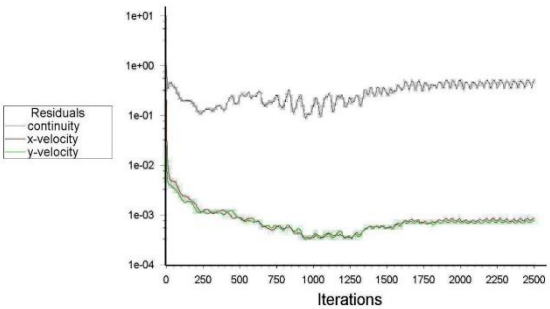

Fig. 7. Residual plot for R_e=7500.

3. Conclusions

Based on observations of the present research it can be claimed that explicit scheme used for primitive variable formulation can be only half the way (as in R_e=2500 for explicit to R_e=5000 for ADI and implicit schemes) as successful as the other two numerical methods due to its relative simplicity. Then again, the limiting Reynolds number for this method can be raised if a finer mesh is used. Comparison of ADI and implicit formulation scheme also reveals that ADI can remain steady with equal Reynolds number of that of implicit formulation, but fails to identify the details of the flow field.

References

[1] E. Erturk, "Discussions on Driven Cavity Flow", *International Journal for Numerical Methods in Fluids*, Vol. 60, No. 3, pp. 275-294, (2009).

[2] M. S. Chandio, M. U. Jhatila, and S. F. Shan, "Finite Element Simulation of Newtonian Lid-Driven Cavity Flow", *Research Journal*, Vol. 45, No. 2, pp. 253-262, (2013).

[3] K. Gustafson, "Four principles of vortex motion", *Vortex Methods and Vortex Motion*, Eds. K. Gustafson and J. Sethian, SIAM Publications, Philadelphia, pp. 95-141, (1991).

[4] Y. F. Peng, Y. H. Shiau, and R. R. Hwang "Transition in a 2-D Lid-Driven Cavity Flow", *Computers and Fluids*, Vol. 32, No. 3, pp. 337-352, (2003).

[5] C. H. Bruneau, and M. Saad, "The 2D Lid Driven Cavity Problem Revisited", *Computers and Fluids*, Vol. 35, No. 3, pp. 326-348, (2006).

[6] U. Ghia, K. N. Ghia, and C. T. Shin, "High-Re Solutions for Incompressible Flow Using the Navier-Stokes Equations and a Multi grid Method", *Journal of Computational Physics*, Vol. 48, No. 3, pp. 387-411, (1982).

[7] E. Barragy, and G. F. Carey, "Stream Function-Vorticity Driven Cavity Solutions Using P-Finite Elements",

Computers and Fluids, Vol. 26, No. 5, pp. 453-468, (1997).

[8] P. S. B. Zdanski, M. A. Ortega, and N. G. C. R. Fico, "Numerical Study of the Flow Over Shallow Cavities", *Computers and Fluids*, Vol. 32, No. 7, pp. 953-974, (2003).

[9] D. S. Kumar, K. S. Kumar, and M. K. Das, "A Fine Grid Solution for a Lid-Driven Cavity Flow Using Multigrid Method", Engineering *Applications of Computational Fluid Mechanics*, Vol. 3, No. 3, pp. 336-354, (2009).

[10] N. P. Moshkin, and K. Poochinapan, "Novel finite difference scheme for the numerical solution of two-dimensional incompressible Navier-Stokes equations", *International Journal Of Numerical Analysis And Modeling*, Vol. 7, No. 2, pp. 321-329, (2010).

[11] K. Poochinapan, "Numerical implementations for 2-d lid-driven cavity flow in stream function formulation", *ISRN Applied Mathematics*, Vol. 2012, Article ID: 871538, 17 pp, (2012).

[12] K. Yapici, and Y. Uludag, "Finite volume simulation of 2-d steady square lid driven cavity flow at high Reynolds numbers", *Brazilian Journal of Chemical Engineering*, Vol. 30, No. 4, pp. 923-937, (2013).

[13] K. M. Salah Uddin, and L. K. Saha, "Numerical solution of 2-d incompressible driven cavity flow with wavy bottom surface", *American Journal of Applied Mathematics*, Vol. 3, No. 1-1, pp. 30-42, (2015).

[14] L. Marioni, F. Bay, and E. Hachem, "Numerical stability analysis and flow simulation of lid-driven cavity subjected to high magnetic field", *Physics of Fluids,* Vol. 28, Article ID 057102, 16 pp, (2016).

[15] D. C. Wan, Y. C. Zhou, and G. W. Wei, "Numerical solution of incompressible flows by discrete singular convolution", *International Journal For Numerical Methods In* Fluids, Vol. 38, No. 8, pp. 789-810, (2002).

[16] B. E. Launder, and D. B. Spalding, "The Numerical Computation of Turbulent Flows", *Computer Methods in Applied Mechanics and Engineering*, Vol. 3, No. 2, pp. 269-289, (1974).

[17] E. Erturk, T. C. Corke, and C. Gokcol, "Numerical Solutions of 2-D Steady Incompressible Driven Cavity Flow at High Reynolds Numbers", *International Journal For Numerical Methods In Fluids*, Vol. 48, No. 7, pp. 747-774, (2005).

[18] E. Erturk, and C. Gokcol, "Fourth Order Compact Formulation of Navier- Stokes Equations and Driven Cavity Flow at High Reynolds Numbers", *International Journal For Numerical Methods In Fluids,* Vol. 50, No. 4, pp. 421-436, (2006).

How to cite this paper:
S. Gharahjeh, A. Ashraf and G. Mahtabi," Comparison of three different numerical schemes for 2D steady incompressible lid-driven cavity flow", *Journal of Computational and Applied Research in Mechanical Engineering*, Vol. 7. No. 2, pp. 151-160

DOI: 10.22061/jcarme.2017.1599.1136

URL: http://jcarme.srttu.edu/?_action=showPDF&article=725